# Accurate Transient Simulation of Interconnects Characterized by Band-Limited Data With Propagation Delay Enforcement in a Modified Nodal Analysis Framework

***S. N. Lalgudi, E. Engin, G. Casinovi and M. Swaminathan***

IEEE Transactions on Electromagnetic Compatibility
vol. 50, no. 3, pp. 715–729, August 2008

## Abstract

A numerical-convolution-based approach has been proposed for the accurate transient simulation of interconnects characterized by band-limited (b.l.) frequency-domain (f.d.) data and terminated by arbitrary equivalent circuits. Propagation delay is enforced in the transient results by obtaining causal impulse responses from b.l.f.d. data, extracting the propagation delays from them, and enforcing the delays in the causal impulse responses. Causal impulse responses are obtained through a new minimum-phase/all-pass decomposition of the frequency data. In this decomposition, a new form for the all-pass component has been proposed that preserves the sign of the original frequency response in the reconstructed response, unlike the prior approaches, leading to an accurate transient result. Arbitrary terminations are conveniently handled by integrating the numerical convolution in a modified nodal analysis (MNA) framework, a framework used by commercial circuit simulators, through a new transient simulation formulation. Numerical results demonstrating the accuracy and capability of the proposed procedure have been presented.

## Copyright Notice

# Accurate Transient Simulation of Interconnects Characterized by Band-Limited Data With Propagation Delay Enforcement in a Modified Nodal Analysis Framework

Subramanian N. Lalgudi, Ege Engin, *Member, IEEE*, Giorgio Casinovi, *Senior Member, IEEE*, and Madhavan Swaminathan, *Fellow, IEEE*

***Abstract*—A numerical-convolution-based approach has been proposed for the accurate transient simulation of interconnects characterized by band-limited (b.l.) frequency-domain (f.d.) data and terminated by arbitrary equivalent circuits. Propagation delay is enforced in the transient results by obtaining causal impulse responses from b.l.f.d. data, extracting the propagation delays from them, and enforcing the delays in the causal impulse responses. Causal impulse responses are obtained through a new minimum-phase/all-pass decomposition of the frequency data. In this decomposition, a new form for the all-pass component has been proposed that preserves the sign of the original frequency response in the reconstructed response, unlike the prior approaches, leading to an accurate transient result. Arbitrary terminations are conveniently handled by integrating the numerical convolution in a modified nodal analysis (MNA) framework, a framework used by commercial circuit simulators, through a new transient simulation formulation. Numerical results demonstrating the accuracy and capability of the proposed procedure have been presented.**

***Index Terms*—Causality, convolution, scattering parameters, signal flow graphs, transient response.**

## I. Introduction

In MANY applications, only the band-limited (b.l.) frequency-domain (f.d.) data (e.g., $S$-, $Y$-, and $Z$-parameters) of an interconnect (e.g., a lossy transmission line) are known. The objective is to perform an accurate transient simulation of the multiport b.l.f.d. data with the port terminations. Such a simulation is useful for studying pulse propagation in a transmission line or for computing crosstalk in coupled transmission lines, when only the $S$-parameters of the lines are known up to a given frequency. In such a simulation, it is of interest: 1) to capture the propagation delay through the interconnects and 2) to conveniently handle arbitrary port terminations.

Most of the prior research in the transient simulation of b.l.f.d. data employ a recursive-convolution-based approach [1]–[6]. However, this approach can become computationally exorbitant for a large number of ports, $N_p$, and/or for a large number of poles, $N_{\rm pl}$ [3]. This computational inefficiency is mainly due to the rational-function fitting procedure required in this approach. Remaining prior research is based on a numerical-convolution-based approach [7]–[13]. This approach does not suffer from the computational inefficiency associated with the rational-function fitting step. Most of the prior research using the numerical-convolution-based approach do not capture the port-to-port propagation delays in the transient simulation, when only the b.l.f.d. data are known about the interconnects [7]–[11]. In the prior research that does capture the propagation delays when only the b.l.f.d. data are known, namely, [12] and [13], arbitrary equivalent circuits for the port terminations cannot be conveniently handled. In this paper, a numerical-convolution-based approach is proposed that not only captures the port-to-port propagation delays but also conveniently handles arbitrary port terminations. Such a handling is accomplished by integrating convolution in a modified-nodal analysis framework, unlike [12] and [13]. The proposed formulation uses a minimum-phase-based reconstruction approach with a sign-preservation term. This extra term, which is missing in [12] and [13], is essential in obtaining accurate transient results in certain examples. Detailed description of the prior research, the contributions of this paper, and the organization of the rest of the paper are provided in Section II.

## II. Background

It has been reported that not enforcing propagation delay (through a causality enforcement) in the transient simulation of interconnects characterized by band-limited data can lead to inaccurate computation of signal integrity quantities like the eye diagram [12], [13]. Based on eye height and width, some interconnect design decisions, like the decision to design a passive equalizer [14], are made. Therefore, it is important to ensure that the propagation delay is enforced in transient simulations of interconnects characterized by b.l.f.d. data. Port terminations are usually described in the form of an equivalent circuit. Since the terminations [in general, can be any simulation program with integrated circuit emphasis (SPICE) circuit] to an interconnect can be arbitrary, it is important that transient simulations of b.l.f.d. data handle arbitrary port terminations and do so with ease.

Manuscript received July 28, 2007; revised November 17, 2007; February 16, 2008.

The authors are with the School of Electrical and Computer Engineering, Georgia Institute of Technology, Altanta, GA 30332 USA (e-mail: gtg228q@mail.gatech.edu; engin@ece.gatech.edu; giorgio.casinovi@ece.gatech.edu; madhavan.swaminathan@ece.gatech.edu).

Color versions of one or more of the figures in this paper are available online at http://ieeexplore.ieee.org.

Digital Object Identifier 10.1109/TEMC.2008.924394

One straightforward approach to perform transient simulation of interconnects such as transmission lines when characterized by b.l.f.d. data is through a physical equivalent circuit-based approach. In this approach, the per-unit-length parameters of the lines are computed from f.d. data, a distributed equivalent circuit of the lines is constructed, SPICE terminations are appended to this equivalent circuit, and the transient simulation is performed through a circuit simulator such as SPICE. Distributed equivalent circuit implicitly accounts for the propagation delay. As commercial circuit simulators such as SPICE can handle arbitrary equivalent circuits, arbitrary terminations are also easily handled. However, this approach has the following shortcomings: 1) a physical equivalent circuit model for the lines is only known in some cases (see [15] for an example) and not in all; 2) distributed modeling significantly increases the run time [5], [16]; and 3) time-domain responses oscillate and show ringing [16]. Therefore, this approach is not preferable for a long lossy transmission line.

In such lossy transmission line applications and in others, the transient simulation of b.l.f.d. data consists of two steps. In the first step, the multiport f.d. data are converted to time-domain multiport impulse responses. In the second step, the port voltages and/or currents are computed from these impulse responses and the port terminations: the multiport impulse responses relate the port quantities, such as the port voltages and the port currents, through convolution. The port terminations enforce an independent set of conditions between the voltage and the current at a port. The second step, therefore, involves solving the convolution relations with the termination conditions. The ease with which arbitrary port terminations are handled depends on how the termination conditions are constructed and solved with the convolution relations.

Depending on how the first step is performed, the existing methods to this transient simulation can be broadly categorized into one of the following two approaches. In the first approach, referred to as the recursive-convolution-based approach [1]–[6], the first step of the transient simulation is accomplished by fitting rational functions to the f.d. data and converting these functions (expressed in pole-residue form) to impulse responses through an inverse laplace transform. This transform is performed analytically, as the poles and residues are already known. Since the poles are known, the convolution can be performed recursively, which scales $O(N_t)$ in time complexity, where $N_t$ is the number of time steps. The computational complexity of the rational-function fitting depends on how many port-to-port responses are fitted simultaneously. When $N_p$ port-to-port responses (out of the total $N_p^2$ responses) are fitted together, the memory and time complexities scale as $O(N_p^2 N_{\mathrm{pl}}^2)$ and $O(N_p^4 N_{\mathrm{pl}}^3)$, respectively, where $N_p$ refers to the number of ports and $N_{\mathrm{pl}}$ to the number of poles. Therefore, the computational complexity of this fitting can get exorbitant when either $N_p$ is large or $N_{\mathrm{pl}}$ is large or both.

In the second approach, referred to as the numerical-convolution-based approach [7]–[13], the first step is accomplished numerically through a simple inverse fast Fourier transform (IFFT) of the f.d. data. Owing to the IFFT, a numerical convolution is employed for the transient simulation. The time complexity of this convolution scales as $O(N_t^2)$. This complexity can be alleviated to $O(N_t \ln N_t)$ through fast convolution methods [13]. The memory and time complexities of the first step scale as $O(N_p^2 N_t)$ and $O(N_p^2 N_t \ln N_t)$, respectively, where $N_t$ refers to the number of time steps. These complexities are very close to optimal values for this step, which is $O(N_p^2 N_t)$ each for memory and time. It is to be noted that these complexities are independent of the nature of the f.d. data, and therefore, are also independent of $N_{\mathrm{pl}}$, unlike the recursive-convolution-based approach. In this paper, owing to the computational effectiveness of the IFFT procedure, numerical-convolution-based approach has been adopted.

However, in a numerical-convolution-based approach, it is difficult to capture the port-to-port propagation delays in the transient simulation. This is because when IFFT is applied to a b.l. data, the resulting time-domain response is usually not causal. A time-domain response is said to be causal if it is zero for $t < 0$. The desired impulse response should, however, be zero for $t < t_p$, where $t_p$ is propagation delay through the system. Such a time-domain response is referred to as delay-causal (in this paper), to differentiate it from a causal response.

Among the prior numerical-convolution-based approaches [7]–[13], [7]–[11] do not capture the propagation delay when only the f.d. data are known about the interconnects. Causal impulse response from a b.l. frequency response in certain microwave applications is obtained through a minimum-phase reconstruction of the original frequency response [17], [18]. The minimum-phase frequency responses are obtained from the magnitude of the f.d. data using the complex cepstrum analysis [19]. For many electromagnetic systems, a nonminimum-phase reconstruction is required [20]–[23]. For long interconnects, a nonminimum-phase reconstruction has been proposed in [12] and [13]. In this new reconstruction, the frequency response is decomposed into a product of a minimum-phase component and an all-pass component. The all-pass component has unity magnitude and is used to model the propagation delay. An exponential form for the all-pass component, $\exp(-j\omega t_p)$, has been employed. Since this form only introduces a time delay to the minimum-phase impulse response, a delay-causal impulse response is naturally obtained. This technique has been applied successfully for uncoupled transmission line problems. The approach in [12] and [13] has two drawbacks that are the subjects of this paper.

The first drawback is that the decomposition in [12] and [13] may not preserve the sign of the original frequency response during reconstruction, i.e., a frequency response $H(\omega) = -1$ would be reconstructed as $H(\omega) = 1$ using this decomposition. When the sign of a port-to-port frequency response is not preserved, the transient results can be inaccurate and sometimes can also be incorrect. The second drawback in [12] and [13] is that it is difficult to handle complicated terminations: in [12] and [13], the transient simulation formulation is based on signal-flow graph-based (SFG-based) approach, proposed in [8]. In an SFG-based approach, the termination conditions are obtained by relating the incident and the reflected waves through the terminations's reflection and transmission coefficients. Computing these coefficients can be easy for simple terminations (such as a resistor

to ground) but can get difficult for complicated terminations (a distributed RLC circuit, for instance), limiting the usefulness of the SFG-based approaches to only simple terminations.

In this paper, a numerical convolution-based procedure for the accurate delay-causal transient simulation of interconnects characterized by b.l.f.d data and terminated by arbitrary equivalent circuits has been proposed. In the proposed procedure, the delay-causality of the impulse response is ensured using a technique similar to the one in [12] and [13]. The difference from [12] and [13] is that a new form of the all-pass component that also preserves the sign of the original frequency response has been proposed. The proposed all-pass component form is $\exp(-j\omega t_p + j\theta)$, where $\theta$ is a constant phase term. This phase, $\theta$, can be used to account for the sign of the frequency response and can be computed numerically from the original frequency response. Also, in the proposed procedure, arbitrary port terminations are handled conveniently using a modified nodal analysis framework [24], a framework used by commercial circuit simulators. In this framework, the termination conditions are expressed through Kirchoff's current and voltage laws, which do not require computing the reflection/transmission coefficients. The preliminary results of the proposed MNA-based simulation are described in [25]. Specifically, in [25], the formulation was presented for simple resistive terminations. In this paper, the formulation in [25] is extended to arbitrary terminations. Improved accuracy of the proposed procedure compared to the prior approach and the commercial circuit simulators Agilent's advanced design software (ADS) and Synopys's HSPICE has been shown.

The contributions of this paper are the following.

1) Numerical-convolution-based delay-causal transient simulation of interconnects characterized by multiport band-limited data that can also conveniently handle arbitrary port terminations.
2) Sign-preserving minimum-phase/all-pass decomposition for the delay-causality enforcement.

The rest of the paper is organized as follows. In Section III, the delay-causality problem with b.l.f.d data has been mathematically formulated. Also, in this section, the procedure to obtain a delay-causal impulse response from the b.l. data using the proposed form for the all-pass component has been described. In Section VI, the numerical convolution-based delay-causal transient simulation procedure has been explained. In Section V, the proposed procedure to handle terminations in an MNA framework has been described. In Section VI, simulation results demonstrating the accuracy of the proposed decomposition and of the proposed transient simulation procedure have been presented. Finally, in Section VII, the conclusions of this paper have been presented.

## III. Delay-Causality Problem

The delay-causality problem solved in this paper, as well as in [12] and [13], can be mathematically stated as follows. Consider a linear time-invariant passive system (the black box in Fig. 1) with an impulse response $h(t)$ and a propagation delay $t_p$. The impulse response $h(t)$ is delay-causal. Let this system be fed by a time-domain signal $x(t)$, and let the time-domain response at the output be $y(t)$. The objective is to find an approximate delay-causal output, $\tilde{y}(t)$, given $x(t)$ and the frequency response (in terms of $Y$-, $Z$-, and $S$-parameters), $H(\omega)$, of the system at uniformly spaced frequency intervals between 0 and $f_c$, where $f_c$ is some high-enough frequency.

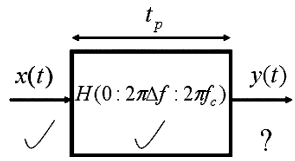


Fig. 1. Definition of the causality problem: Given $x(t)$ and the band-limited and sampled frequency data, $H(\omega)$, of a passive system with a propagation delay, $t_p$, find the output $y(t)$ such that $t_p$ is strictly enforced in $y(t)$; $\Delta f$ is the frequency step of the sampled data, and $f_c$ is some high-enough frequency up to which the data is known. A tick mark indicates a known (or given) quantity, and the question mark indicates an unknown quantity to be computed.

Since $x(t)$ and $y(t)$ are related through convolution, $\tilde{y}(t)$ can be computed, if an approximate delay-causal impulse response, $\tilde{h}(t)$, can be found (see [12] and [13]). If $\hat{h}(t)$ denotes the inverse fourier transform (IFT) of the b.l. response $H(0:2\pi\Delta f:2\pi f_c)$, where $\Delta f$ is the frequency step, then $\hat{h}(t)$ is not the preferred solution, as $\hat{h}(t)$ is not delay-causal [12], [13]. This is because when $f_c$ is finite [equivalent to multiplying the infinite frequency response $H(0:2\pi\Delta f:\infty)$ by a gate function of width $f_c$], $\hat{h}(t)$ is actually the convolution of a time-domain sinc function, which is noncausal, and $h(t)$, which is delay-causal, Therefore, $\hat{h}(t)$ can be nondelay-causal and may be noncausal too. Then, the objective is to find an $\tilde{h}(t)$ that approximates $h(t)$ from only $H(0:2\pi\Delta f:2\pi f_c)$.

In the rest of the section, the procedure in [12] and [13] to obtain the delay-causal impulse response from b.l. data has been briefly explained, followed by the description of a possible limitation of this procedure in preserving the sign of the original frequency response. Next, a new decomposition for the frequency response that removes this limitation has been proposed.

### A. Delay-Causal Impulse Response Using Linear-Phase Condition

In [12] and [13], a decomposition procedure for $H(\omega)$ that results in a $\tilde{h}(t)$ has been presented. This decomposition is given as

$$H(\omega) = H_{\min}(\omega)\, e^{-j\omega t_p} \tag{1}$$

where $H_{\min}(\omega)$ is the minimum-phase component (see [19] and [26]). The function $H_{\min}(\omega)$ is the delayless part of $H(\omega)$ and models effects due to attenuation and dispersion. The term $e^{-j\omega t_p}$ is the all-pass component, which has been used to model the phase using a linear-phase condition. The term $t_p$ here refers to the propagation delay if $H(\omega)$ was lossless. For a lossy transmission line of length $l$, $t_p$ would mean the propagation delay of a lossless line of the same length and is calculated by the value of the propagation delay at $\omega = \infty$ [23].

The IFT of the b.l. response $H_{\min}(0:\omega_c)$, $\hat{h}_{\min}(t)$, is causal (see [19]). Therefore, the IFT of the right-hand side (RHS) of

(1), $\hat{h}_{\min}(t-t_p)$, is delay-causal. Therefore, $\tilde{h}(t)$ is chosen as

$$\tilde{h}(t) = \hat{h}_{\min}(t-t_p). \tag{2}$$

The component $H_{\min}(\omega)$ in (1) is computed from the magnitude of $H(\omega)$

$$|H_{\min}(\omega)| = |H(\omega)| \tag{3}$$

$$\arg[H_{\min}(\omega)] = -\mathrm{HT}\{\ln|H(\omega)|\}. \tag{4}$$

In (3) and (4), $|x|$ stands for the magnitude of $x$, $\arg[x]$ is the principal argument of complex number $x$, and $\mathrm{HT}\{x\}$ is the Hilbert transform [19] of $x$. Using a discrete Hilbert transform [19], (4) can be rewritten as

$$\arg[H_{\min}(\omega)] = -\frac{1}{2\pi}\mathcal{P}\int_{\theta=-\pi}^{\pi} \ln|H(\theta)| \cot\left(\frac{\omega-\theta}{2}\right) d\theta \tag{5}$$

where $\mathcal{P}$ denotes the Cauchy principal value of the integral that follows. In [12] and [13], the delay $t_p$ in (1) is computed as

$$t_p = -\text{Average Slope}\left(\arg\left[\frac{H(\omega)}{H_{\min}(\omega)}\right]\right). \tag{6}$$

Propagation delay computed in the average sense (6) works well when there is just a single delay in the frequency response. When more than one delay is present in the frequency response, like in a dispersive transmission line where the velocity is a function of frequency, then $t_p$ calculated from (6) is an approximation. For a more accurate $t_p$, $t_p$ should be computed as the smallest delay in the response.

Extra computational cost is incurred in obtaining a delay-causal response, $\tilde{h}(t)$, as opposed to a nondelay-causal response, $\hat{h}(t)$. These operations include those required to obtain $H_{\min}(\omega)$ (3), (5), those required to obtain $t_p$ (6), and those required to obtain $\hat{h}(t)$ (2). Among these, obtaining the discrete Hilbert transform [i.e., (5)] is the most expensive. Two Fourier transform operations are needed in implementing (5) (see [19]), which can be performed efficiently using IFFT. Therefore, asymptotic computational complexity in obtaining a delay-causal impulse response is the same as that for a nondelay-causal impulse response.

### B. Limitation of Linear-Phase Condition

The procedure thus far described works as long as $H(\omega)$ can be decomposed according to the functional form described in (1). However, when $H(\omega)$ has a constant negative sign, a simple example is $H(\omega) = -1$, the decomposition in (1) is not sufficient. The off-diagonal terms of the admittance matrix of a resistive circuit have the form $H(\omega) = -g$, where $g > 0$ is the conductance between the two different ports.

To see the insufficiency of (1), $H(\omega) = -g$ is reconstructed using (1). From (3), $|H_{\min}(\omega)| = g$. From the property of Hilbert transforms, the Hilbert transform of a constant is zero [27]. This can also be proven from (5) by deducing that for a constant $H(\omega)$, the integrand is an odd function. Therefore, the integration result is zero. Using this fact in (4), $\arg[H_{\min}(\omega)] = 0$. Therefore, $H_{\min}(\omega) = g$.

Since in a resistive circuit, there is no propagation delay between ports, $t_p = 0$. Therefore, the exponential term in (1), call it $H_{\mathrm{ap}}(\omega)$, is 1.

From $H_{\min}(\omega) = g$ and $H_{\mathrm{ap}}(\omega) = 1$, the original response $H(\omega) = -g$ is reconstructed as only $g$ using the decomposition in (1)! In fact, since only the magnitude of $H(\omega)$ is used to compute $H_{\min}(\omega)$, all frequency responses of the form $H(\omega) = ge^{j\theta}$ will be reconstructed as just $g$, where $\theta$ is a constant real number. This disparity in the phase between the original frequency response and the reconstructed frequency response could affect the accuracy of the transient results, as will be shown in Section VI.

### C. Delay-Causal Impulse Response Using Generalized Linear-Phase Condition

To account for a constant phase term in the frequency response, the form of the decomposition in (1) is modified as

$$H(\omega) = H_{\min}(\omega)\, e^{-j\omega t_p + j\theta}. \tag{7}$$

For the example $H(\omega) = -g$, $\theta = \pm\pi$. Therefore, using (7), $H(\omega) = -g$ can be reconstructed from $H_{\min}(\omega) = g$, $t_p = 0$, and $\theta = \pi$. Therefore, the proposed all-pass component form is $e^{-j\omega t_p + j\theta}$. The resulting condition on the phase of the all-pass component is referred to as the generalized linear-phase condition, a condition used to denote a generalized linear-phase system (see [19, p. 295]).

The constant phase $\theta$ in (7) can be computed numerically from the frequency data by 1) equating the phases of the left-hand side (LHS) and the RHS of (7), and 2) solving for $\theta$ from the resulting equation, which can be written as

$$\theta = \arg[H(\omega)] - \arg[H_{\min}(\omega)] - \arg\left[e^{-j\omega t_p}\right]. \tag{8}$$

The phase $\theta$ from (8) can be computed by obtaining the RHS at any $\omega$ or by calculating the average of the RHS's for all $\omega$'s. However, it has to be noted that $t_p$ is only computed in the average sense in Section III-A, and hence, can contribute to some inaccuracy while calculating the term $\omega t_p$ in (8). This inaccuracy issue can be avoided if $\theta$ is computed by obtaining the RHS at $\omega = 0$. However, computing $\theta$ at $\omega = 0$ is not reliable for the following reason: At $\omega = 0$, the magnitude of the transfer response can be zero, making the angle of the response zero too at $\omega = 0$. Such a case arises in coupled transmission lines. Also, the angle of the minimum-phase response at $\omega = 0$ is always zero. For $\omega = 0$, the integrand in (5) is an odd function of $\theta$. Therefore, at $\omega = 0$, $\theta$ can be computed to be zero. Therefore, the phase $\theta$ is computed near $\omega = 0$. If the angle of the original frequency response or of its minimum-phase component is discontinuous near $\omega = 0$, then this angle is computed in the asymptotic sense (value of the angle as $\omega \to 0$).

Irrespective of the $\omega$ at which $\theta$ is computed, there are some restrictions on the values $\theta$ can take. The term $e^{j\theta}$ (7) introduces a constant phase change to the rest of the response for all frequencies including $\omega = 0$. Since $H(0)$ and $H_{\min}(0)$ are both real, the term $e^{j\theta}$ can only be a real number. Therefore, the phase angle $\theta$ can take values among 0, $\pi$, and $-\pi$ rad. These

values mean that the term $e^{j\theta}$ at the most can result in (and account for) a sign change.

With the proposed decomposition in (7), the impulse response $\tilde{h}(t)$ in (2) is computed differently, as the IFT of the RHS of (7), i.e.,

$$\tilde{h}\,(t) = \hat{h}_{\min,\theta}\,(t - t_p) \tag{9}$$

where $\hat{h}_{\min,\theta}\,(t)$ is the b.l. IFT of the product $H_{\min}\,(\omega)\,e^{j\theta}$.

## IV. Numerical Convolution-Based Delay-Causal Transient Simulation

Using (9), all the impulse responses between two different ports are obtained as delay-causal impulse responses. However, the impulse responses between the same ports (i.e., $s_{ii}(t), y_{ii}(t)$, etc.) are obtained as the IFT of the corresponding frequency responses, as is being done in [12] and [13]. This different treatment to the self-terms is due to the following considerations: 1) The self-impulse responses represent the reflection (or return loss) characteristics at a port due to an excitation at the same port. As there is no delay between the same ports, propagation delays for self-terms are made zero. In the case of multiple delays, the smallest of them is zero. 2) Port-to-port frequency responses between the same ports are considered as minimum phase [20], and minimum-phase frequency responses have a causal time-domain response [19]. Therefore, self-impulse responses are automatically delay-causal with a delay of zero.

Once the multiport impulse responses are known, the transient simulation involves computing the port voltages given the equivalent circuits of the port terminations. For a numerically robust transient simulation, the f.d. data are expressed as $S$-parameters [9]. The transient simulation requires solving the convolution equations relating the port quantities, such as the incident and reflected waves, with the equations describing the termination conditions. In the rest of the section, the convolution equations are derived.

Let $\overline{\overline{S}}\,(\omega) \in \mathbf{C}^{N_p \times N_p}$ be the multiport $S$-parameter. Then, $\overline{\overline{S}}\,(\omega)$ can be written as

$$\overline{\overline{S}}\,(\omega) = \overline{\overline{S}}\,(\infty) + \overline{\overline{\hat{S}}}\,(\omega) \tag{10}$$

where $\overline{\overline{S}}\,(\infty)$ is $\overline{\overline{S}}\,(\omega)$ at $\omega = \infty$ and is due to the direct coupling between the input and the output ports, and $\overline{\overline{\hat{S}}}\,(\omega)$ is the remaining part of $\overline{\overline{S}}\,(\omega)$. If $\bar{A}\,(\omega) \in \mathbf{C}^{N_p \times 1}$ and $\bar{B}\,(\omega) \in \mathbf{C}^{N_p \times 1}$, respectively, are the vectors of incident and reflected waves [38], then $\bar{B}\,(\omega) = \overline{\overline{S}}\,(\omega)\,\bar{A}\,(\omega)$, which in the time domain becomes

$$\bar{b}\,(t) = \bar{\bar{s}}\,(t) * \bar{a}\,(t)\,. \tag{11}$$

In (11), $\bar{\bar{s}}\,(t)$, $\bar{a}\,(t)$, and $\bar{b}\,(t)$ are the IFTs of $\overline{\overline{S}}\,(\omega)$, $\bar{A}\,(\omega)$, and $\bar{B}\,(\omega)$, respectively. The symbol "*" in (11) denotes a linear convolution [19] and is defined as

$$y(t) = h\,(t) * x\,(t) = \int_{\tau=0}^{t} h\,(t-\tau)x\,(\tau)\,d\tau. \tag{12}$$

If $h(t)$ in (12) does not have any impulses, then the continuous integration in (12) can be discretized using a (right) rectangular integration rule as

$$y\,(t) \approx \sum_{m=1}^{n} h\,((n-m)\,\Delta t)\,x\,(m\Delta t)\,\Delta t + O(\Delta t) \tag{13}$$

where $\Delta t$ is the time step, and $O(\Delta t)$ denotes the first-order accuracy of the integration rule. Defining $\bar{\bar{\hat{s}}}\,(t)$ to be the IFT of $\overline{\overline{\hat{S}}}\,(\omega)$ and $\delta\,(t)$ to be the Dirac-Delta function, $\bar{\bar{s}}\,(t)$ can be written as

$$\bar{\bar{s}}\,(t) = \overline{\overline{S}}\,(\infty)\,\delta\,(t) + \bar{\bar{\hat{s}}}\,(t)\,. \tag{14}$$

Making use of (12)–(14), (11) can be written as

$$\bar{b}\,(t) \approx \overline{\overline{S}}\,(\infty)\,\bar{a}\,(t) + \sum_{m=1}^{n} \bar{\bar{\hat{s}}}\,((n-m)\,\Delta t)\,\bar{a}\,(m\Delta t)\Delta t. \tag{15}$$

When the $n$th term in the summation in (15) is separated and combined with the first term of the RHS of (15), then the resulting equation can be rewritten as

$$-\left[\overline{\overline{S}}\,(\infty) + \bar{\bar{\hat{s}}}\,(0)\,\Delta t\right]\bar{a}\,(t) + \bar{b}\,(t) = \bar{h}\,(t) \tag{16}$$

where

$$\bar{h}\,(t) = \sum_{m=1}^{n-1} \bar{\bar{\hat{s}}}\,((n-m)\,\Delta t)\,\bar{a}\,(m\Delta t)\,\Delta t. \tag{17}$$

From (17), it can be observed that $\bar{h}(t)$ depends only on the known values of $\bar{a}$; hence, the RHS of (16) is known. However, $\bar{a}\,(t)$ and $\bar{b}\,(t)$ in (16) are still not known. Therefore, (16) constitutes a set of $N_p$ equations with $2N_p$ unknowns [both $\bar{a}(t)$ and $\bar{b}(t)$]. The system in (16) has be solved together with the equations describing the terminations.

## V. Handling Terminations

In this section, the procedure to handle port terminations in SFG-based approaches [8], [12], [13] has been briefly explained, followed by a description of its limitation to handle complicated terminations. Next, the MNA-based convolution simulation that handles terminations without the limitations in an SFG-based approach has been proposed.

### A. Handling Terminations in an SFG-Based Approach

Since both $\bar{a}\,(n\Delta t)$ and $\bar{b}\,(n\Delta t)$ are still not known in (16), at least another $N_p$ equations are needed to compute them. The additional $N_p$ equations are obtained by relating $\bar{a}\,(t)$ and $\bar{b}\,(t)$ through the termination conditions [8]

$$\bar{a}\,(t) = \overline{\overline{\Gamma}}\,(t)\,\bar{b}\,(t) + \overline{\overline{\mathrm{T}}}\,(t)\,\bar{g}\,(t)\,. \tag{18}$$

In (18), $\overline{\overline{\Gamma}}\,(t) \in \mathbf{R}^{N_p \times N_p}$ and $\overline{\overline{\mathrm{T}}}\,(t) \in \mathbf{R}^{N_p \times N_p}$ are the diagonal matrices of the reflection and the transmission coefficients at the ports at time $t$, respectively. The vector $\bar{g}\,(t) \in \mathbf{R}^{N_p \times 1}$ is a function of the excitations at the ports and is known at time $t$. The port quantities $\bar{a}\,(t)$ and $\bar{b}\,(t)$ can now be obtained by solving (16) together with (18). Let $N_n$ denote the total number

of nodes in the network, and let the first $N_p$ nodes correspond to the $N_p$ ports. If $\overline{v}(t) \in \mathbf{R}^{N_n \times 1}$ denotes the vector of node voltages, then the port voltages can be computed as

$$\overline{v}_{1:N_p}(t) = \overline{a}(t) + \overline{b}(t). \tag{19}$$

In [12] and [13], the port voltages at every time step are computed by solving (16), (18), and (19) . The disadvantage of such a computation is that the matrices $\overline{\overline{\Gamma}}(t)$ and $\overline{\overline{\mathrm{T}}}(t)$ in (18) are difficult to compute when the terminations have complicated equivalent circuits, as computing these matrices require computing driving point impedances looking away from the ports.

### *B. Handling Terminations in an MNA-Based Approach*

This difficulty can be avoided if the termination conditions in (18) are alternatively enforced through a modified nodal analysis formulation. If $\overline{i}(t) \in \mathbf{R}^{N_p \times 1}$ is the vector of currents entering the ports, then the MNA of the whole network (multiport network + rest of the network) yields the following system of equations:

$$\overline{\overline{C}}\,\dot{\overline{x}}(t) + \overline{\overline{G}}\,\overline{x}(t) + \begin{bmatrix} \overline{i}(t) \\ \overline{0}_{N_{\mathrm{mna}}-N_p} \end{bmatrix} = \overline{r}(t) \tag{20}$$

where

$$\dot{\overline{x}}(t) = \frac{d\overline{x}(t)}{dt}, \quad \overline{x}(t) \in \mathbf{R}^{N_{\mathrm{mna}} \times 1}$$

is the vector of unknown variables in an MNA approach, and $\overline{r}(t) \in \mathbf{R}^{N_{\mathrm{mna}} \times 1}$ is a vector describing the current and the voltage sources in the whole network. The quantities $\overline{\overline{C}} \in \mathbf{R}^{N_{\mathrm{mna}} \times N_{\mathrm{mna}}}$ and $\overline{\overline{G}} \in \mathbf{R}^{N_{\mathrm{mna}} \times N_{\mathrm{mna}}}$, $\overline{r}(t) \in \mathbf{R}^{N_{\mathrm{mna}} \times 1}$ have the same definitions as in the MNA approach, and $N_{\mathrm{mna}} = N_n + N_{v_s} + N_L$. The symbol $N_{v_s}$ denotes the total number of voltage sources in the network, and the symbol $N_L$ denotes the total number of inductors in the network. In (20), the symbol $\overline{0}_k$ denotes a column vector of zeros with $k$ rows.

Since $\overline{i}(t)$ in (20) is dependent on the f.d. data, the MNA system in (20) cannot be solved alone. Assuming all ports are referenced with respect to a characteristic admittance of $Y_0 \in \mathbf{R}$, the port currents can be expressed as

$$\overline{i}(t) = Y_0\left(\overline{a}(t) - \overline{b}(t)\right). \tag{21}$$

When $\overline{i}(t)$ in (21) is substituted in (20), the latter equation can be rewritten as

$$\overline{\overline{C}}\,\dot{\overline{x}}(t) + \overline{\overline{G}}\overline{x}(t) + Y_0\begin{bmatrix} \overline{a}(t) \\ \overline{0}_{N_{\mathrm{mna}}-N_p} \end{bmatrix} - Y_0\begin{bmatrix} \overline{b}(t) \\ \overline{0}_{N_{\mathrm{mna}}-N_p} \end{bmatrix} = \overline{r}(t). \tag{22}$$

To solve for all the node voltages including the port voltages, (22) is solved along with (16) and (19). The system combining these equations can be written as

$$\overline{\overline{W}}\,\dot{\overline{u}}(t) + \overline{\overline{V}}\,\overline{u}(t) = \overline{z}(t) \tag{23}$$

where $\overline{u}(t) \in \mathbf{R}^{N_{\mathrm{mna}}+2N_p \times 1}$, $\overline{\overline{W}} \in \mathbf{R}^{N_{\mathrm{mna}}+2N_p \times N_{\mathrm{mna}}+2N_p}$, $\overline{\overline{V}} \in \mathbf{R}^{N_{\mathrm{mna}}+2N_p \times N_{\mathrm{mna}}+2N_p}$, and $\overline{z}(t) \in \mathbf{R}^{N_{\mathrm{mna}}+2N_p \times 1}$. These quantities are defined as follows:

$$\overline{u}(t) = \begin{bmatrix} \overline{x}(t) \\ \overline{a}(t) \\ \overline{b}(t) \end{bmatrix} \tag{24}$$

$$\overline{\overline{W}} = \begin{bmatrix} \overline{\overline{C}} & \overline{\overline{0}}_{N_{mna} \times 2N_p} \\ \overline{\overline{0}}_{2N_p \times N_{mna}} & \overline{\overline{0}}_{2N_p \times 2N_p} \end{bmatrix} \tag{25}$$

$$\overline{\overline{V}} = \begin{bmatrix} \overline{\overline{G}} & Y_0\overline{\overline{I}}_{N_p} & -Y_0\overline{\overline{I}}_{N_p} \\ \overline{\overline{0}}_{N_p \times N_{\mathrm{mna}}} & -\left(\overline{\overline{S}}(\infty) + \overline{\overline{\hat{s}}}(0)\,\Delta t\right) & \overline{\overline{I}}_{N_p} \\ \overline{\overline{I}}_{N_p} & \overline{\overline{0}}_{N_p \times N_{\mathrm{mna}}-N_p} & \overline{\overline{I}}_{N_p} \end{bmatrix} \tag{26}$$

$$\overline{z}(t) = \begin{bmatrix} \overline{r}(t) \\ \overline{h}(t) \\ \overline{0}_{N_p} \end{bmatrix}. \tag{27}$$

In (25) and (26), the symbol $\overline{\overline{0}}_{m \times n}$ denotes a matrix of zeros with $m$ rows and $n$ columns, and $\overline{\overline{I}}_m$ denotes an identity matrix of size $m$. The unknown node voltages ($\overline{u}_{1:N_p}(t)$) can be computed from the solution of (23). The system (23) has the same form as the system most SPICE-like simulators (see [24] and [28]) have. Therefore, numerical techniques to solve (23) are the same as those employed in SPICE-like simulators. With the formulation described thus far, any linear termination can be handled without having to compute the reflection or the transmission coefficients at the ports.

The proposed formulation can also be extended to nonlinear terminations. It is to be noticed that when the terminations are linear, (23) would represent a system of linear algebraic equations. This linear system of equations can be solved using linear matrix solution techniques. On the other hand, if the terminations are nonlinear, (20) [therefore, even (22)] would have nonlinear terms in addition to the existing terms, as part of the MNA of the nonlinear elements. Equation (23) would therefore represent a system of nonlinear algebraic equations, which can be solved using the Newton–Raphson method [29].

The explicit splitting of $\overline{\overline{S}}(\omega)$ described in (10) can be avoided by dividing the $S$-parameters by $\Delta t$ before computing the impulse response from them and by using IFFT [19] to obtain the impulse responses: Defining $\overline{\overline{p}}(t)$ to be the IFFT [19] ($\neq$ IFT. Note IFFT and IFT results can differ by a factor of $\Delta t$) of $\frac{\overline{\overline{S}}(\omega)}{\Delta t}$, $\overline{\overline{p}}(t)$ can be expressed as

$$\overline{\overline{p}}(t) = \frac{\overline{\overline{S}}(\infty)}{\Delta t}\delta(t) + \overline{\overline{\hat{s}}}(t). \tag{28}$$

From (28), the following can be inferred:

$$\overline{\overline{S}}(\infty) + \overline{\overline{\hat{s}}}(0)\,\Delta t = \overline{\overline{p}}(0)\,\Delta t \tag{29}$$

$$\overline{\overline{\hat{s}}}(t \neq 0) = \overline{\overline{p}}(t \neq 0). \tag{30}$$

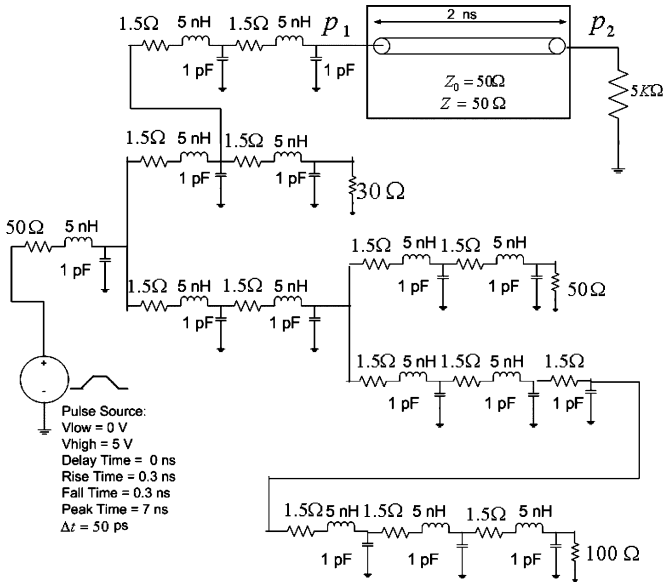


Fig. 2. Test setup for computing pulse response of a lossless transmission line terminated by a distributed RLC circuit. The transmission line is characterized by band-limited two-port causal $S$-parameters from 0 to 10 GHz with a frequency step of 1 MHz.

Using (29) and (30) in (16), it can be observed that (16) can be rewritten only in terms of $\overline{\overline{p}}\,(t)$, which is obtained without any splitting to $\overline{\overline{S}}\,(\omega)$.

## VI. Results

In this section, simulation results demonstrating the accuracy of the proposed decomposition in (7) and of the proposed transient simulation procedure have been presented. For demonstrating accuracy, Agilent's ADS [30], Synopsys's HSPICE [31], frequency-domain solutions have been used as references. The ADS engine is based on the numerical-convolution-based approach. The HSPICE engine ($W$-element $w/$ $S$-parameter input) is based on the recursive-convolution-based approach. Further, in HSPICE simulations, delay is extracted first before rational-function fitting. Group delay is used for this purpose.

First, the accuracy of the proposed method in handling complicated terminations and in extracting the propagation delay is demonstrated. For this demonstration, an example is chosen such that the decomposition in (1) alone is sufficient for the reconstruction of the frequency response. As an example, the pulse response of a lossless transmission line (see Fig. 2) is considered. The propagation delay in this line is 2 ns. The average delay extracted using (6) is also 2 ns. The source termination in Fig. 2 is an example of the kind of termination for which it is difficult to use an SFG-based approach, as it is difficult to compute the Thevenin's equivalent circuit for the source. On the other hand, in the MNA-based approach, no such difficulty is present. The voltages at both the near end and the far end of the line (ports $p_1$ and $p_2$ in Fig. 2) are computed using both delay-causal and nondelay-causal impulse responses. For a lossless transmission line and for an available bandwidth $f_c = k(1/t_p)$, where $t_p$ is the propagation delay, and $k$ is a positive integer, the nondelay-causal impulse response is automatically delay-causal. That is, in such a situation, no explicit delay extraction and enforcement is needed. Therefore, for this example ($f_c = 20(1/t_p)$), the nondelay-causal results are the most accurate with respect to handling the f.d. data. To compare the accuracy of the whole system, which includes even the terminations, ADS and HSPICE are used. For this example, the ADS results are expected to be delay-causal for the same reason mentioned earlier. Therefore, both ADS and HSPICE results can be reliable reference solutions. The delay-causal (denoted as "Delay-Causal") and nondelay-causal voltages ("Nondelay-Causal") are compared with those obtained from ADS ("ADS") and from HSPICE ("HSPICE") in Fig. 3(a)–(c). From Fig. 3(a)–(c), it can be observed that the "Delay-Causal" results from the proposed procedure match closely with the other results. From Fig. 3(c), it can be observed that propagation delay (= 2 ns) is captured exactly in the 'Delay-Causal' results. This example demonstrates the accuracy of the proposed formulation in handling complicated terminations and in extracting (and enforcing) the propagation delay.

Next, the accuracy of the proposed transient simulation has been demonstrated for a dispersive transmission line characterized by a causal data. As an example, the pulse response of a lossy strip line [see Fig. 4(a)] is considered. The product of the frequency-dependent inductance and capacitance is shown in Fig. 4(b). A lossless stripline of the same length would have a delay of approximately 6.47 ns. The average delay extracted using (6) is 6.5 ns. The voltages at both the near end and the far end of the line are computed using both delay-causal and nondelay-causal impulse responses. These voltages are compared with those obtained from ADS and HSPICE in Fig. 5(b)–(d). Unlike the previous example, the transmission line is lossy. Therefore, it is not possible to exploit periodicity to get a reference solution. Therefore, the "Nondelay-Causal" results may not be reliable as a reference solution with respect to handling the f.d. data. Therefore, the problem was also solved in the frequency domain, and the frequency-domain voltages are converted to the corresponding time-domain results using the IFFT. Since the IFFT results inherently denote a circular convolution, care has been taken to make these results perform a linear convolution (see [19, p. 580, Fig. 8.18]). The IFFT results are used as the reference. From Fig. 5(a) and (b), it can be observed that the "Delay-Causal" and "Nondelay-Causal" results from the proposed procedure match closely with the results from both ADS and IFFT. However, the propagation delay (= 6.5 ns) is captured in the "Delay-Causal" (proposed) results [see Fig. 5(c)] but not in the "Nondelay-Causal" and "ADS" results. It is to be noted that the nondelay-causal formulation is the same as the delay-causal formulation except for the delay extraction and enforcement in the latter. This comparison shows that unless the propagation delay is extracted and enforced explicitly, it is usually not captured. It is to be noted that the IFFT results will not capture the propagation delay, as these results are equivalent to performing a linear convolution without the delay enforcement. Therefore, the IFFT results would be similar to the nondelay-causal results in terms of delay enforcement and accuracy. This example demonstrates the accuracy of the proposed formulation in handling dispersive causal data.

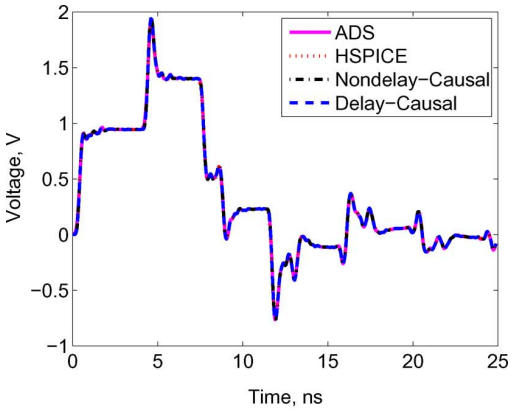


(a)

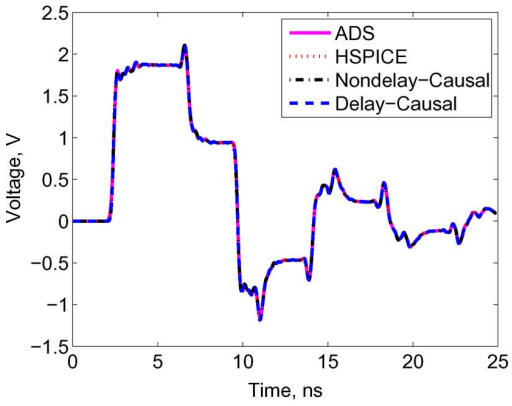


(b)

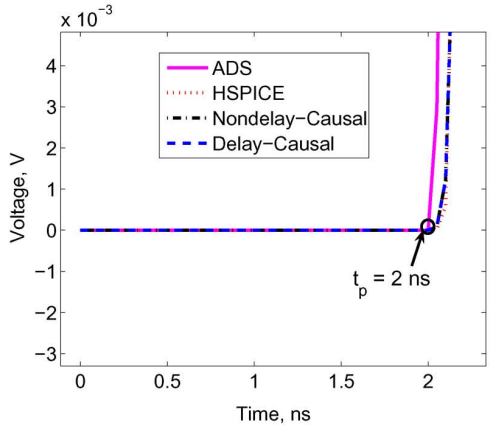


(c)

Fig. 3. Comparison of pulse responses at $p_1$ and $p_2$ in Fig. 2 between the proposed method ("Delay-Causal") and ADS, HSPICE, and nondelay-causal simulations. (a) Voltage at the near end of the transmission line, i.e., at $p_1$ in Fig. 2. (b) Voltage at the far end of the transmission line, i.e., at $p_2$ in Fig. 2. (c) Zoomed-in voltage at the far end of the transmission line between 0 and 2 ns. Note the propagation delay of 2 ns through the line is captured in the "Delay-Causal" results.

The "Delay-Causal" results are also compared with "HSPICE" results in the same figure [Fig. 5(a)–(c)]. It is to be noted that the HSPICE results are different from the rest of the results in two ways: 1) From Fig. 5(a) and (b), it can be noticed that the HSPICE results are inaccurate compared to the rest of the results. This inaccuracy is due to the approximation

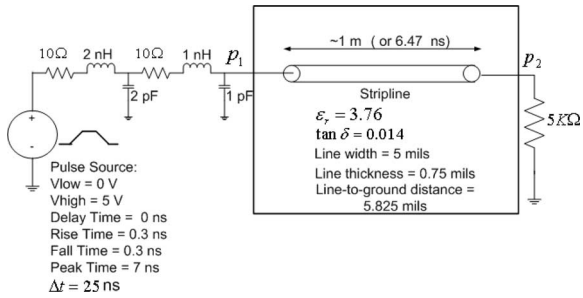


(a)

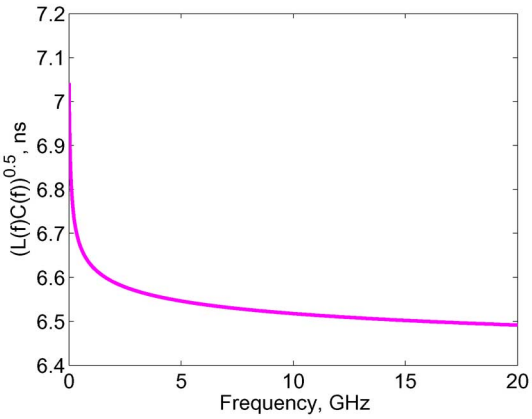


(b)

Fig. 4. Test setup of pulse response of a lossy transmission line terminated by a distributed RLC circuit. The transmission line is characterized by band-limited two-port causal $S$-parameters from 0 to 20 GHz with a frequency step of 1 MHz. (a) Test setup. (b) Square root of the product of frequency-dependent inductance and capacitance.

involved in fitting a rational function system to delayless frequency responses. On the other hand, "Delay-Causal" results do not suffer from this inaccuracy, as they are obtained using a numerical-convolution-based approach (which does not curvefit responses). 2) From Fig. 5(c), it can be noticed that the propagation delay from HSPICE (6.775 ns) is approximately 0.275 ns ($= 11\Delta t$) more than the predicted delay. From the "IFFT" and "Nondelay-Causal" results in Fig. 5(c), it can be inferred that the propagation delay of more than 6.5 ns may not be an accurate solution. Therefore, the proposed method can be more accurate than recursive-convolution-based approaches like the $W$-element in HSPICE in some situations.

In the previous example, the amplitudes of the nondelay-causal responses before the propagation delay were small (see "Nondelay-Causal," "ADS," and "IFFT" results in Fig. 5 for $t < 6.5$ ns). This has to do with the causal nature of the data. However, if the S-parameters were noncausal, this amplitude can be significant [6]. Though the use of noncausal data is not advised [6], there are situations when the user is not aware of the causality of the data. For example, some existing transmission line models (see TLINP model in ADS) inherently produce noncausal data. The proposed technique can be used to get an approximate causal time-domain response given even some noncausal data. This feature is demonstrated in the next example. It is to be noted that Hilbert-transform-based techniques have

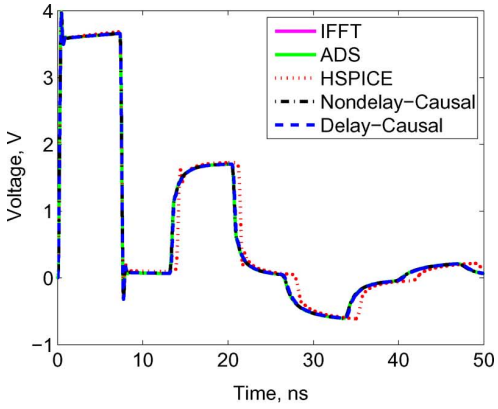


(a)

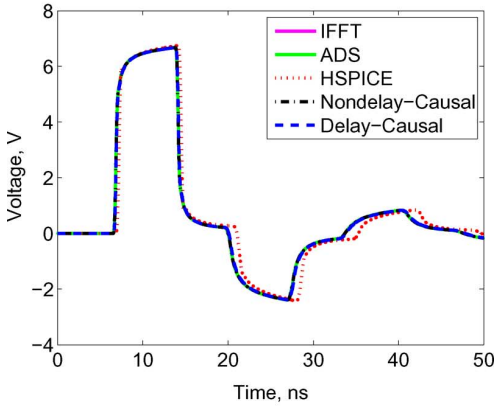


(b)

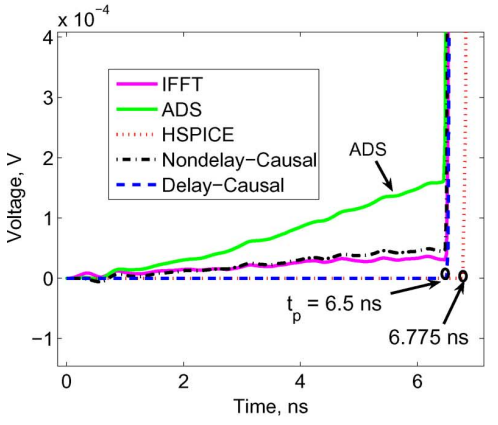


(c)

Fig. 5. Comparison of pulse responses of the setup in Fig. 4 between the proposed method ("Delay-Causal") and ADS, HSPICE, frequency-domain solution ("IFFT"), and nondelay-causal simulations. (a) Voltage at the near end of the transmission line, i.e., at $p_1$ in Fig. 4. (b) Voltage at the far end of the transmission line, i.e., at $p_2$ in Fig. 4. (c) Zoomed-in voltage at the far end of the transmission line between 0 and 7 ns. Note the propagation delay of 6.5 ns through the line is captured in the "Delay-Causal" results only.

been employed in the past to handle noncausal data (see [26] and [32]–[36]). The previous example is repeated for a new transmission line specification (see Fig. 6). The noncausal data were obtained by a noncausal circuit model that considers variation in $R(f)$ and $G(f)$ but ignores variation in $L(f)$ and $G(f)$ (see the model TLINP in ADS). The actual propagation delay for this line is 3 ns. The average delay extracted using (6) is also 3 ns. As can be observed from Fig. 7(c), the "Delay-Causal" results capture the propagation delay ($=$ 3 ns), while the other two results do not. Also, from Fig. 7(c), it can be observed that the amplitudes of the nondelay-causal voltages ("Nondelay-Causal" and "ADS") before the propagation delay are not small. The close match between the "Nondelay-Causal" results and "ADS" results in Fig. 7(a) and (b) demonstrates the accuracy of the proposed formulation without the delay enforcement. The difference observed between the "ADS" and the "Delay-Causal" results is due to using noncausal data without delay-causality enforcement in the former.

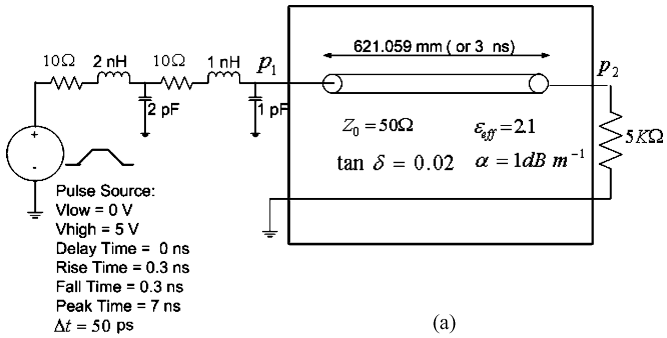


(a)

Fig. 6. Pulse response of a lossy transmission line terminated by a distributed RLC circuit. The transmission line is characterized by band-limited two-port noncausal $S$-parameters from 0 to 10 GHz with a frequency step of 1 MHz. (a) Test setup.

The "Delay-Causal" results in Fig. 7(a), (c) are also compared with those from HSPICE in Fig. 8(a)–(c). From Fig. 8(a) and (b), it can be observed that the "Delay-Causal" results match very closely with the "HSPICE" results. Also, from Fig. 8(c), it can be noticed that propagation delay is captured in both the results. The reason for this close agreement with HSPICE is attributed to the delay extraction done prior to rational-function fitting in HSPICE [31]. Such a processing in HSPICE is similar to the one followed in the method-of-characterisics approach [6]. This approach has been demonstrated to yield delay-causal responses for lossy transmission lines in [6].

Until now, the decomposition in (1) is sufficient for all the examples. To demonstrate the need for and the accuracy of the proposed decomposition in (7), a coupled-line example is considered. As an example, the step response in two coupled transmission lines is simulated. Consider the symmetric lossless coupled microstrip transmission lines shown in Fig. 9. The geometry of the lines and of the substrate are specified in Fig. 9. The coupled lines are modeled by four-port $S$-parameters from 0 to 4 GHz (Agilent's ADS was used for obtaining the $S$-parameters). At port $p_1$, a step voltage source is applied. All the ports are terminated with $Z_0$ ($=$ 22 Ω). It was found that the decomposition in (7) was needed only for the transfer response $S_{41}$. This need would be felt if the constant phase $\theta$ in (7) is shown to take a nonzero value (if $\theta = 0$, the proposed decomposition in (7) is the same as the decomposition in (1), hence there is no need for the proposed decomposition). Therefore, the phase $\theta$ is computed for $S_{14}$ ($= S_{41}$), using the numerical procedure described in Section III-C.

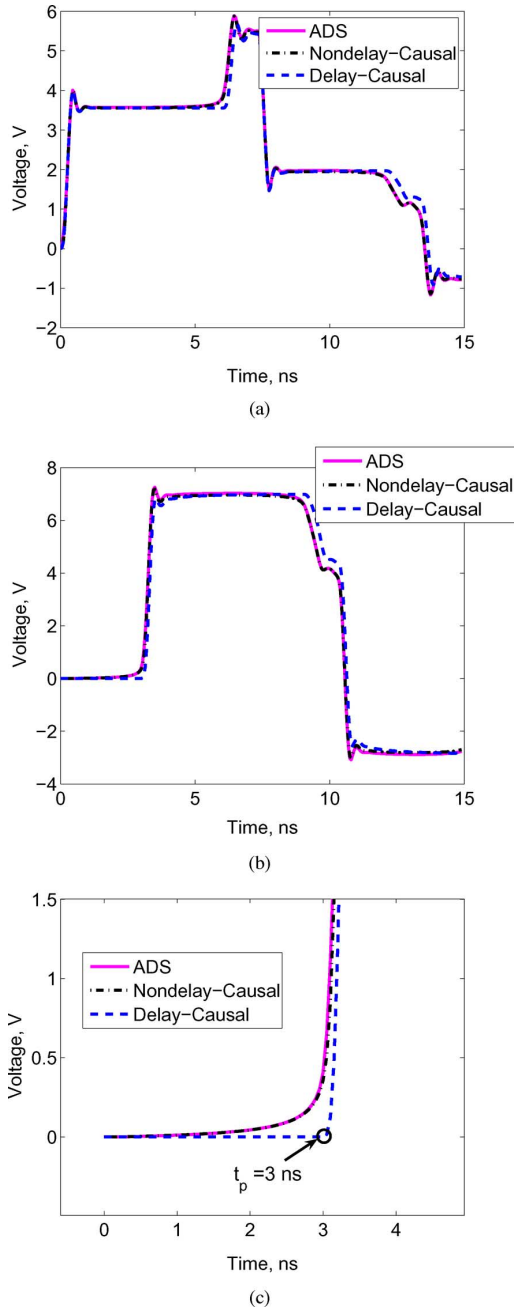


Fig. 7. Comparison of pulse responses of the setup in Fig. 6 between the proposed method ("Delay-Causal") and ADS and nondelay-causal simulation. (a) Voltage at the near end of the transmission line, i.e., at $p_1$ in Fig. 6. (b) Voltage at the far end of the transmission line, i.e., at $p_2$ in Fig. 6. (c) Zoomed-in voltage at the far end of the transmission line between 0 and 4 ns. Note the propagation delay of 3 ns through the line is captured in the "Delay-Causal" results only.

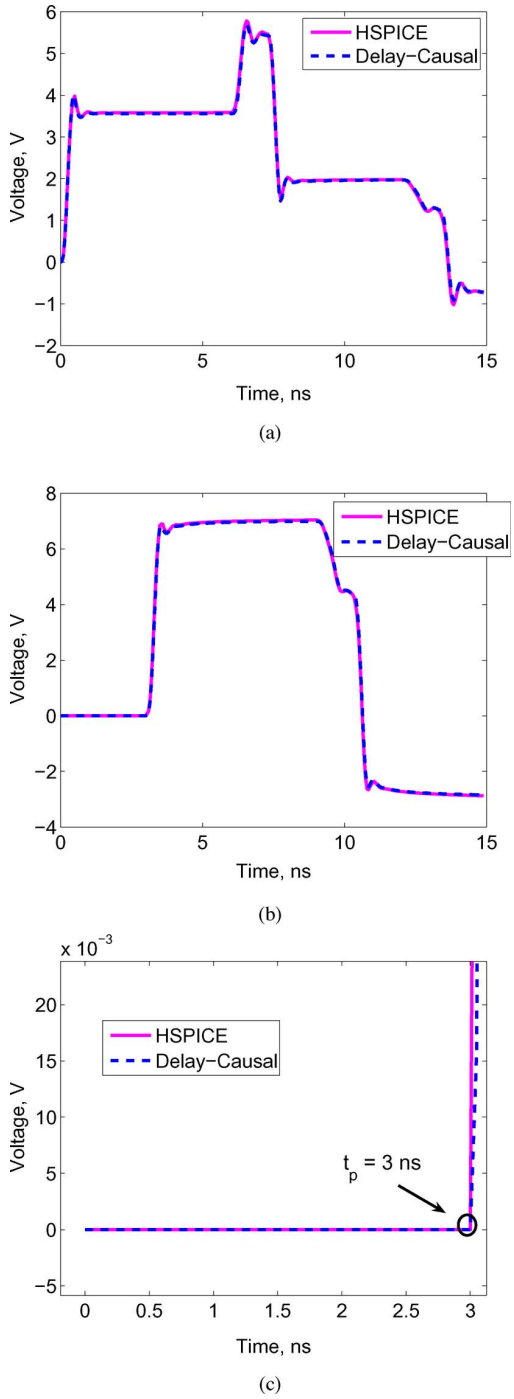


Fig. 8. Comparison of pulse responses of the setup in Fig. 6 between the proposed method ("Delay-Causal") and HSPICE. (a) Voltage at the near end of the transmission line, i.e., at $p_1$ in Fig. 6. (b) Voltage at the far end of the transmission line, i.e., at $p_2$ in Fig. 6. (c) Zoomed-in voltage at the far end of the transmission line between 0 and 4 ns. Note the propagation delay of 3 ns through the line is captured in the "Delay-Causal" results only.

The numerical phase extraction procedure in Section III-C requires computing the angles of the original frequency response and of the minimum-phase response near $\omega \approx 0$ [see (8) specifically]. This procedure is described next. In Figs. 10 and 11, the procedures to compute the angle of the $S_{14}$ and of its minimum-phase component near $\omega = 0$, respectively, are described. Fig. 10 consists of two parts: 1) in the first part, the angle of $S_{14}(\omega)$ is shown for frequencies up to 4 GHz and 2) in the second part, the angle of $S_{14}(\omega)$ is shown only for frequencies near $f = 0$. (See only the results from "ADS" for the current discussion; the discussion on the "Analytical" results are deferred for now.) From the second part of Fig. 10, it can be observed that $\arg[S_{14}(f)] \to -\pi/2$ as $f \to 0$.

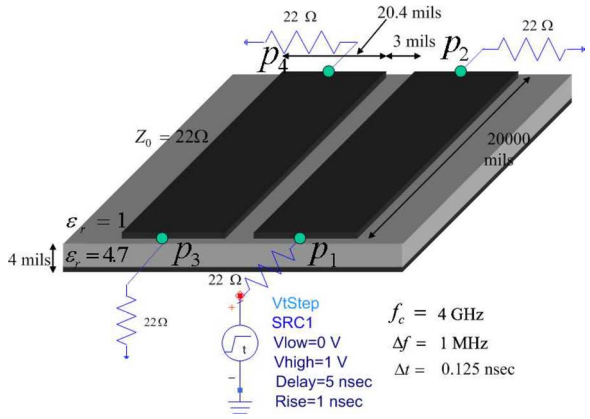


Fig. 9. Test setup of a coupled microstrip transmission line circuit in which the lines are characterized by four-port $S$-parameters. The symbol $p_i$ refers to port $i$. The circuit is excited by a step source at $p_1$, and the transient voltages at $p_2$ and $p_4$ are computed.

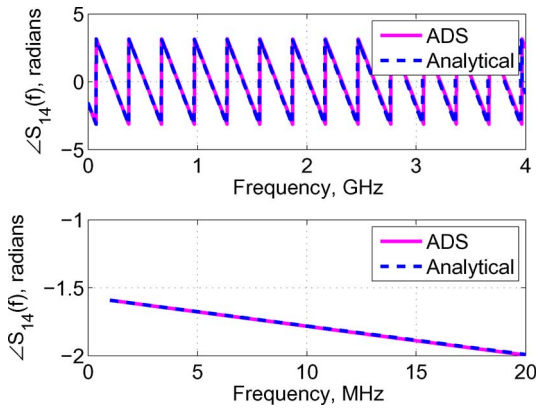


Fig. 10. $\arg[S_{14}(f)] \to -\pi/2$ as $f \to 0$.

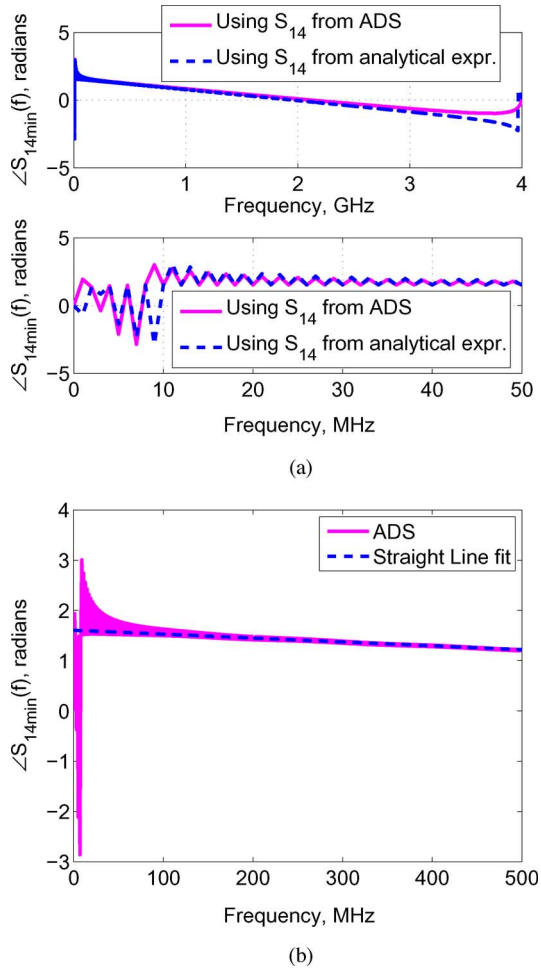


Fig. 11. $\arg[S_{14\min}(f)] \to \pi/2$ as $f \to 0$. (a) Angle of $S_{14_{\min}}(f)$ as a function of $f$. (b) Straight-line fit to calculate the angle of the minimum-phase component $f \to 0$.

In Fig. 11, the procedure to compute the phase of $S_{14\min}(\omega)$ near $\omega = 0$ is described. Once again, in Fig. 11, the discussion on "$\cdots$ analytical expr." is deferred for now. Unlike $\arg[S_{14}(f)]$, $\arg[S_{14\min}(f)]$ is not smooth near $f = 0$ (see both parts of Fig. 11). The argument of $S_{14\min}(f)$ is found to have numerical oscillations (triangular oscillations with period $2\Delta f$, see Fig. 11) because only a numerical Hilbert transform is being applied and the phase of minimum-phase component changes abruptly at $f = 0$. Hence, an asymptotic value of the phase is computed for $S_{14\min}(f)$. It is found that $\arg[S_{14\min}(f)] \to \frac{\pi}{2}$ asymptotically as $f \to 0$, as shown in Fig. 11(b) by the intercept of the straight line (fitted to the angle of the minimum-phase response) with $f = 0$ axis. Since the angles $\arg[S_{14}(f)]$ and $\arg[S_{14\min}(f)]$ approach different values as $f \to 0$, it is obvious from (8) that $\theta \neq 0$ for $S_{14}(\omega)$. Using these phases and using (8), the constant phase $\theta$ is computed to be $-\pi$ for $S_{14}(f)$.

This value of $\theta$ for $S_{14}(\omega)$ can be verified theoretically as follows. The discussion deferred thus far on the analytical results in Figs. 10 and 11 is now explained. From [37], $S_{14}(\omega)$ can be analytically expressed as

$$S_{14}(\omega) = -je^{-j\beta_0 l}\sin((\beta_e - \beta_o)\, l) \tag{31}$$

where $l$ is the length of the line, and $\beta_0$ is the propagation constant of the uncoupled line, and $\beta_e$ and $\beta_o$ are the even- and odd-mode propagation constants of the coupled lines. These propagation constants are defined as

$$\beta_0 = \frac{\omega\varepsilon_{\text{eff}}^{\frac{1}{2}}}{c} \quad \beta_e = \frac{\omega\varepsilon_e^{\frac{1}{2}}}{c} \quad \beta_o = \frac{\omega\varepsilon_o^{\frac{1}{2}}}{c}$$

where $c$ is the velocity of light in vacuum, $\varepsilon_{\text{eff}}$ is the effective relative dielectric constant of the lines when they are uncoupled, and $\varepsilon_e$ and $\varepsilon_o$ are the even- and odd-mode relative dielectric constants, respectively, of the lines when they are coupled. For the coupled line in Fig. 9, $\varepsilon_{\text{eff}}$ can be computed as 3.9056 from [38]; the dielectric constants $\varepsilon_e$ and $\varepsilon_o$ are obtained from ADS and are 4.191 and 3.604, respectively. To validate the expression in (31), the plots in Figs. 10 and 11 are obtained using (31) and are plotted together with the previous plots. From (31), because of the term $-j$, it can be clearly seen that $\arg[S_{14}(f)] \to -\pi/2$ as $f \to 0$. Also, from (31) and (4), $S_{14_{\min}}(f) = -\Im\{\text{HT}\{\ln|\sin((\beta_e - \beta_o)\, l)|\}\}$, for which there is no analytical solution. It can be numerically shown that the argument of the minimum-phase response of a sine function

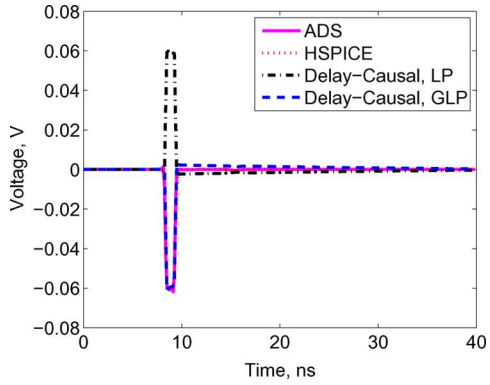


Fig. 12. Comparison of transient results at $p_4$ in Fig. 9 using the decompositions in (1) ("Delay-Causal, LP") and (7) ("Delay-Causal, GLP").

such as $\sin(a\omega)$, where $a$ is independent of $\omega$, approaches $\frac{\pi}{2}$ asymptotically as $f \to 0$. Therefore, the constant phase $\theta = -\pi$ for $S_{14}(\omega)$.

With the need for the decomposition in (7) already established, the effect of using (or not using) the proposed decomposition on the transient results is shown next. The objectives of the following are twofold: 1) to further demonstrate the need for the proposed decomposition using transient results and 2) to demonstrate the accuracy of the proposed transient simulation procedure with the proposed decomposition. The effect on the transient results can be considerable sometimes, as will be shown in the current example, and can be not-so considerable yet important sometimes, as will be shown in the next example. For this purpose, the voltage at $p_4$ (see Fig. 9) is computed. In Fig. 12, the voltages at $p_4$ obtained from the decomposition in (1) ("Delay-Causal, LP" in Fig. 12) and from the decomposition in (7) ("Delay-Causal, GLP" in Fig. 12) are compared. The voltages from ADS and from HSPICE are used as a reference. From Fig. 12, it can be observed that the voltage in the case "Delay-Causal, LP" differs in sign from the voltage in the case "Delay-Causal, GLP." Thus, not using the proposed decomposition can result in an incorrect transient result.

In the previous example, the correct result among the results obtained with and without the decomposition could be found with the knowledge of the far-end crosstalk due to a step source. In the next example, a case is shown where such finding would be hard. As an example, the coupled lines in Fig. 9 are excited at $p_1$ and $p_3$ by pseudorandom bit sources, and the voltages at all the ports are computed. Each source has a series resistance of 0.25 Ω, an amplitude of 5 V, and a rise and fall time of 0.5 ns. The time step of the simulation is the same as in the previous example. In Fig. 13, the voltages at all the four ports are compared with those from ADS and HSPICE. From Fig. 13(b) and (d), it can be seen that the results from the case "Delay-Causal, GLP" (dash) match with those from ADS (solid) and HSPICE (dot), demonstrating the accuracy of the transient results with the proposed decomposition. It can be noticed that the voltages at $p_4$ ($p_3$) from the case "Delay-Causal, LP" (dash–dot) have opposite voltage excursions compared to the voltages from the other cases. The difference between the cases "Delay-Causal, LP" and "Delay-Causal, GLP" is not as considerable as it was in

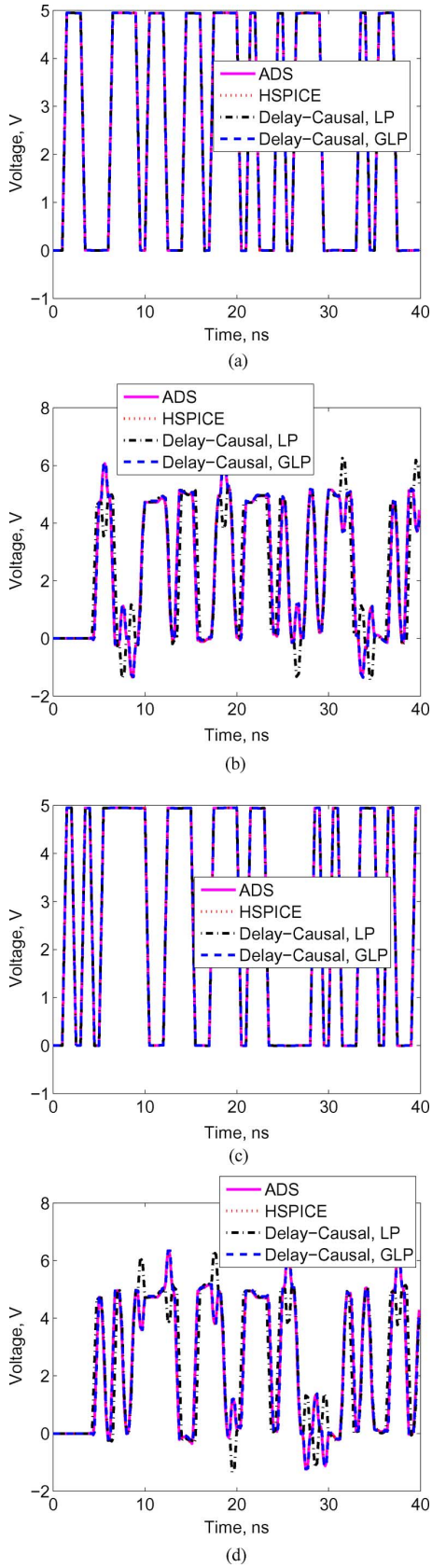


Fig. 13. Comparison of transient responses obtained with linear-phase condition and with generalized linear-phase condition. Example is a coupled transmission line excited by pseudorandom bit patterns. (a) Voltage at $p_1$. (b) Voltage at $p_2$. (c) Voltage at $p_3$. (d) Voltage at $p_4$.

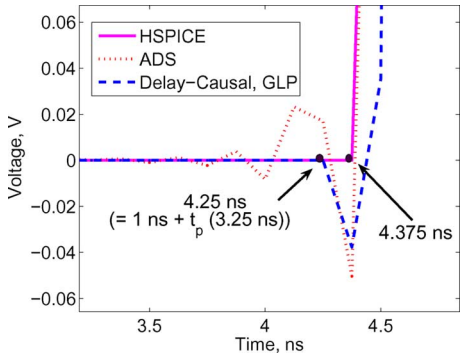


Fig. 14. Comparison of voltage at $p_4$ between 3.5 and 4.5 ns from different methods. Approximate propagation delay is captured in the delay-causal result.

the previous example, yet may be important. Moreover, this difference can become considerable if the rise time of the voltage source is reduced, as the crosstalk is inversely proportional to rise time in a two-coupled transmission line [39]. Therefore, the proposed decomposition in (7) is necessary for accurate delay-causal transient simulation in examples such as the coupled transmission lines.

Though the "Delay-Causal" results match well with ADS [Fig. 13(a)–(d)], the propagation delay is captured only in the former. To demonstrate this difference, the voltage at $p_4$ is compared between the "Delay-Causal" and "ADS" results for 3.5–4.5 ns in Fig. 14. The propagation delays computed with $\epsilon_{\text{eff}}$, $\epsilon_e$, and $\epsilon_o$ are 3.349, 3.469, and 3.217 s, respectively. The average delay computed from (6) is 3.2713 s for $S_{41}(f)$. The sources at $p_1$ and $p_3$ are nonzero only after 1 ns. Therefore, the voltage at $p_4$ should be nonzero only after an additional time delay equal to the propagation delay. From Fig. 14, it can be observed that the propagation delay (approximated to the nearest multiple of $\Delta t$ in Fig. 14) is captured in the "Delay-Causal" result but not in the "ADS" result. The HSPICE result has an approximate propagation delay of 3.375 ns (see Fig. 14).

The proposed method, unlike the $W$-element in HSPICE, can be theoretically applied to even nontransmission line examples.

## VII. Conclusion

A numerical-convolution-based procedure has been proposed for the accurate transient simulation of interconnects characterized by band-limited frequency-domain data and terminated by arbitrary equivalent circuits. Propagation delay is enforced in the transient results by obtaining a causal impulse response through a new minimum-phase/all-pass decomposition of the frequency data, extracting the delay from the data, and enforcing the delay in the causal impulse response. In this decomposition, a new form for the all-pass component has been proposed that preserves the sign of the original frequency response in the reconstructed response, unlike the prior approaches, leading to an accurate transient result. This new form is shown to be essential in computing the far-end crosstalk in coupled microstrip transmission lines. Arbitrary terminations are conveniently handled by integrating the numerical convolution in a modified nodal analysis framework, a framework used by commercial circuit simulators, through a new transient simulation formulation. Numerical results demonstrating the improved accuracy and capability of the proposed procedure compared to the prior approach and to the commercial circuit simulators Agilent's advanced design software and Synopsys's HSPICE have been shown.

## Acknowledgment

The authors would like to thank M. Tsuk from Ansoft Corporation for providing data for one of the examples. The authors would also like to thank the anonymous reviewers for their suggestions toward improving the quality of this manuscript.

## References

[1] S. Lin and E. S Kuh, "Transient simulation of lossy interconnects based on a recursive convolution formulation," *IEEE Trans. Circuits Syst. I: Fundam. Theory Appl.*, vol. 39, no. 11, pp. 879–892, Nov. 1992.

[2] W. T. Beyene and J. E. Schutt-Aine, "Efficient transient simulation of high-speed interconnects characterized by sampled data," *IEEE Trans. Compon. Packag. Manuf. Technol. B*, vol. 21, no. 1, pp. 105–114, Feb. 1998.

[3] S. Min, "Automated construction of macromodels from frequency data for simulation of distributed interconnect networks" Ph.D. disseration, Dept. Elect. Comput. Eng., Georgia Inst. Technol., Atlanta, GA, 2004.

[4] D. Saraswat, R. Achar, and M. Nakhla, "Global passivity enforcement algorithm for macromodels of interconnect subnetworks characterized by sampled data," *IEEE Trans. Very Large Scale Integr. (VLSI) Syst.*, vol. 13, no. 7, pp. 819–832, Jul. 2005.

[5] A. Dounavis, N. Nakhla, R. Achar, and M. Nakhla, "Delay extraction and passive macromodeling of lossy coupled transmission lines," in *Proc. IEEE Conf. Elect. Perform. Electron. Packag.*, Oct, 2003, pp. 251–254.

[6] S. Grivet-Talocia, H. M. Huang, A. E. Ruehli, F. Canavero, and I. M. Elfadel, "Transient analysis of lossy transmission lines: An efficient approach based on the method of characteristics," *IEEE Trans. Adv. Packag.*, vol. 27, no. 1, pp. 45–56, Feb. 2004.

[7] A. R. Djordevic and T. K. Sarkar, "Transient analysis of electromagnetic systems with multiple lumped nonlinear loads," *IEEE Trans. Antennas Propag.*, vol. AP-33, no. 5, pp. 533–539, May 1985.

[8] J. E. Schutt-Aine and R. Mittra, "Scattering parameter transient analysis of transmission lines loaded with nonlinear terminations," *IEEE Trans. Microw. Theory Tech.*, vol. MTT-36, no. 3, pp. 529–536, Nov. 1988.

[9] D. Winklestein, M. B. Steer, and R. Pomerleau, "Simulation of arbitrary transmission line networks with nonlinear terminations," *IEEE Trans. Circuits Syst.*, vol. 38, no. 4, pp. 418–422, Apr. 1991.

[10] L. P. Vakanas, A. C. Cangellaris, and O. A. Palusinski, "Scattering parameter-based simulation of transients in lossy nonlinearly terminated packaging interconnections," *IEEE Trans. Compon. Packag. Manuf. Technol. B*, vol. 17, no. 4, pp. 472–479, Nov. 1994.

[11] M. S. Basel, M. B. Steer, and P. D. Franzon, "Simulation of high speed interconnects using a convolution-based hierarchical simulator," *IEEE Trans. Compon. Packag. Manuf. Technol. B*, vol. 18, no. 1, pp. 74–82, Feb. 1995.

[12] R. Mandrekar and M. Swaminathan, "Causality enforcement in transient simulation of passive networks through delay extraction," in *Proc. 9th IEEE Workshop Signal Propag. Interconnects*, May 2005, pp. 25–28.

[13] R. Mandrekar, K. Srinivasan, E. Engin, and M. Swaminathan, "Causal transient simulation of passive networks with fast convolutionin," in *Proc. 10th IEEE Workshop Signal Propag. Interconnects*, May, 2006, pp. 61–64.

[14] K. J. Han, H. Takeuchi, E. Engin, and M. Swaminathan, "Eye-pattern improvement for design of high-speed differential links using passive equalization," in *Proc. 15th IEEE Conf. Elect. Perform. Electron. Packag.*, Nov., 2006, pp. 241–244.

[15] X. Shi, J. G. Ma, K. S. Yeo, M. A. Do, and E. Li, "Equivalent circuit model of on-wafer CMOS interconnects for RFICs," *IEEE Trans. Very Large Scale Integr. (VLSI) Syst.*, vol. 13, no. 9, pp. 1060–1071, Sep. 2005.

[16] W. T. Beyene and C. Yuan, "An accurate analysis of high-speed package interconnects using convolution technique," *IEEE Trans. Analog Integr. Circuits Signal Process.*, vol. 35, no. 2–3, pp. 107–120, May.–Jun. 2003.
[17] P. Perry and T. J. Brazil, "Hilbert-transform-derived relative group delay," *IEEE Trans. Microw. Theory Tech.*, vol. 45, no. 8, pp. 1214–1225, Aug. 1997.
[18] P. A. Perry and T. J. Brazil, "Forcing causality on $S$-parameter data using the Hilbert transform," *IEEE Trans. Microw. Guided Wave Lett.*, vol. 8, no. 11, pp. 378–380, Nov. 1998.
[19] A. Oppenheim and R. Schafer, *Discrete-Time Signal Processing*, 2nd ed. Englewood Cliffs, NJ: Prentice-Hall, 1999.
[20] T. K. Sarkar, "Generation of nonminimum phase from amplitude-only data," *IEEE Trans. Microw. Theory Tech.*, vol. 46, no. 8, pp. 1079–1084, Aug. 1998.
[21] J. Koh and T. K. Sarkar, "Reconstruction of the non-minimum phase function from amplitude only data," in *Proc. IEEE Microw. Symp. Dig. MTT-S*, Jun., 2000, vol. 2, pp. 1093–1096.
[22] J. Yang, J. Koh, and T. K. Sarkar, "Reconstructing a non-minimum phase response from the far-field power pattern of an electromagnetic system," *Proc. IEEE Microw. Symp. Dig. MTT-S*, vol. 53, no. 2, pp. 833–841, Feb. 2005.
[23] H. Curtins and A. V. Shah, "Pulse behavior of transmission lines with dielectric losses," *IEEE Trans. Circuits Syst.*, vol. CAS-32, no. 8, pp. 819–826, Aug. 1985.
[24] H. Chung-Wen, A. E. Ruehli, and P. A. Brennan, "The modified nodal analysis approach to network analysis," *IEEE Trans. Circuits Syst.*, vol. CAS-22, no. 6, pp. 504–509, Jun. 1975.
[25] S. N. Lalgudi, K. Srinivasan, G. Casinovi, R. Mandrekar, E. Engin, Y. Kretchmer, and M. Swaminathan, "Causal transient simulation of systems characterized by frequency-domain data in a modified nodal analysis framework," in *Proc. 15th IEEE Conf. Elect. Perform. Electron. Packag.*, Nov., 2006, pp. 123–126.
[26] F. M. Tesche, "On the use of the Hilbert transform for processing measured CW data," *IEEE Trans. Electromagn. Compat.*, vol. 34, no. 3, pp. 259–266, Aug. 1992.
[27] S. L. Hahn, *Hilbert Transforms in Signal Processing*, 2nd ed. Norwood, MA: Artech House, 1996.
[28] L. T. Pillage, R. A. Rohrer, and C. Visweswariah, *Electronic Circuit and System Simulation Methods*, New York: McGraw-Hill, 1994.
[29] K. S. Kundert, *The Designer's Guide to SPICE & SPECTRE*. Norwell, MA: Kluwer, 1995.
[30] *Agilent Advanced Design System User's Guide*, Agilent Technologies, Santa Rosa, CA, 2006.
[31] *HSPICE Simulation and Analysis User Guide*, Version Y-2006.03, Synopsys Inc. Mountain View, CA, Mar. 2006.
[32] J. R. James and G. Andrasic, "Assessing the accuracy of wideband electrical data using Hilbert transforms," in *Proc. IEEE Proc. Microw. Antennas Propag.*, Jun., 1990, vol. 137, no. 3, pp. 184–188.
[33] T. R. Arabi, A. T. Murphy, and T. K. Sarkar, "An efficient technique for the time-domain analysis of multi-conductor transmission lines using the Hilbert transform," in *Proc. IEEE MTT-S Dig.*, Jun., 1992, vol. 1, pp. 185–188.
[34] T. R. Arabi and R. Suarez-Gartner, "Time domain analysis of lossy multiconductor transmission lines using the Hilbert transform," in *Proc. IEEE MTT-S Dig.*, Oct., 1993, vol. 2, pp. 987–990.
[35] S. M. Narayana, G. Rao, R. Adve, T. K. Sarkar, V. C. Vannicola, M. C. Wicks, and S. A. Scott, "Interpolation/extrapolation of frequency-domain responses using the Hilbert transform," *IEEE Trans. Microw. Theory Tech.*, vol. 14, no. 10, pp. 1621–1627, Oct. 1996.
[36] P. Triverio and S. Grivet-Talocia, "Causality-constrained interpolation of tabulated frequency responses," in *Proc. IEEE MTT-S Dig., 15th IEEE Conf. Elect. Perform. Electron. Packag.*, Nov., 2006, pp. 181–184.
[37] D. A. Hill, K. H. Cavcey, and R. T. Johnk, "Crosstalk between microstrip transmission lines," *IEEE Trans. Electromagn. Compat.*, vol. 36, no. 4, pp. 314–321, Nov. 1994.
[38] D. M. Pozar, *Microwave Engineering*, 3rd ed. New York: Wiley, 2005.
[39] C. R. Paul, "Solution of the transmission-line equations under the weak-coupling assumption," *IEEE Trans. Electromagn. Compat.*, vol. 44, no. 3, pp. 413–423, Aug. 2002.

**Subramanian N. Lalgudi** received the B.E. degree in electronics and communication engineering from Anna University, Chennai, India, in 1999, and the M.S. degree in electrical engineering from Iowa State University, Ames, in 2003. He is currently working toward the Ph.D. degree in electrical engineering at the Georgia Institute of Technology, Atlanta.

From July 1999 to July 2000, he was a Software Engineer in Future Software Pvt. Ltd., Chennai, where he was engaged in the implementation of data networking protocols. From August 2000 to August 2002, he was a Research Assistant in the Department of Electrical and Computer Engineering, Iowa State University. From August 2002 to December 2002, he was a Visiting Scholar in the Department of Electrical and Computer Engineering, Michigan State University, East Lansing. From January 2003 to May 2003, he was a Teaching Assistant in the Department of Electrical and Computer Engineering, Iowa State University. Since August 2003, he has been a Research Assistant in the Department of Electrical and Computer Engineering, Georgia Institute of Technology. His current research interests include numerical methods, computational electromagnetics, fast algorithms, parasitic extraction, circuit simulation, macromodeling, interconnect analysis, and signal and power integrity.

Mr. Lalgudi is a Reviewer for the IEEE TRANSACTIONS on ELECTROMAGNETIC COMPATIBILITY.

**Ege Engin** received the B.S. degree in 1998 from Middle East Technical University, Ankara, Turkey, and the M.S. degree in 2001 from the University of Paderborn, Paderborn, Germany, both in electrical engineering, and the Ph.D. degree in electrical engineering (*summa cum laude*) from the University of Hannover, Hannover, Germany.

From 2001 to 2004, he was with the Fraunhofer Institute for Reliability and Microintegration, Berlin, Germany. Since 2005, he has been with the Packaging Research Center, Georgia Institute of Technology, Atlanta. He is the author or coauthor of more than 50 publications in journals and conferences in the areas of signal and power integrity modeling and simulation. He is the coauthor of *Power Integrity Modeling and Design for Semiconductors and Systems* (Prentice-Hall, 2007). His current research interests include mixed-signal design, characterization, and test.

Dr. Engin is a Reviewer for the IEEE TRANSACTIONS ON ELECTROMAGNETIC COMPATIBILITY.

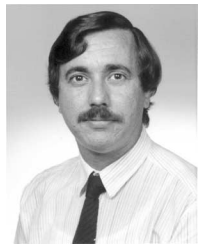

**Giorgio Casinovi** (M'89–SM'93) received the B.S. degrees in electrical engineering and mathematics from the University of Rome, Rome, Italy, in 1980 and 1982, respectively, and the M.S. and Ph.D. degrees in electrical engineering from the University of California, Berkeley.

Since 1989, he has been with the School of Electrical and Computer Engineering, Georgia Institute of Technology, Atlanta. His current research interests include computer-aided design and simulation of electronic devices, circuits, and mixed-technology systems.

**Madhavan Swaminathan** (A'91–M'95–SM'98–F'06) received the B.E. degree in electronics and communication from the University of Madras, Chennai, India, and the M.S. and Ph.D. degrees in electrical engineering from Syracuse University, Syracuse, NY.

He is a Co-Founder of Jacket Micro Devices, where he has been associated as a Chief Scientist. He has also been with the Advanced Packaging Laboratory at IBM, where he was engaged in research on packaging for supercomputers. He is currently the Joseph M. Pettit Professor in Electronics in the School of Electrical and Computer Engineering, Georgia Institute of Technology, Atlanta, and the Deputy Director of the Packaging Research Center. He is the author or coauthor of more than 300 publications in refereed journals and conferences, and three book chapters. He is the author of *Power Integrity Modeling and Design for Semiconductors and Systems* (Prentice-Hall, 2007) and Co-Editor of *Introduction to SOC, SIP, and SOP* (McGraw-Hill, 2008). He is the holder of 15 issued patents and has several patents pending. His current research interests include mixed signal microsystem and nanosystem integration.

Prof. Swaminathan served as the Co-Chair for the 1998 and 1999 IEEE Topical Meeting on Electrical Performance of Electronic Packaging (EPEP), served as the Technical and General Chair for the International Microelectronics and Packaging Society (IMAPS) Next Generation IC & Package Design Workshop, serves as the Chair of TC-12, the Technical Committee on Electrical Design, Modeling, and Simulation within the IEEE Components Packaging and Manufacturing Technology (CPMT) Society, and was the Co-Chair for the 2001 IEEE Future Directions in IC and Package Design Workshop. He is the Co-Founder of the International Microelectronics and Packaging Society (IMAPS) Next Generation IC & Package Design Workshop and the IEEE Future Directions in IC and Package Design Workshop. He also serves on the technical program committees of the Design Automation Conference (DAC), Electrical Performance of Electronic Packaging (EPEP), Signal Propagation on Interconnects (SPI) Workshop, Solid State Devices and Materials Conference (SSDM), Electronic Components and Technology Conference (ECTC), and International Symposium on Quality Electronic Design (ISQED). He has been a Guest Editor for the IEEE TRANSACTIONS ON ADVANCED PACKAGING and the IEEE TRANSACTIONS ON MICROWAVE THEORY AND TECHNIQUES. He was an Associate Editor of the IEEE TRANSACTIONS ON COMPONENTS and PACKAGING TECHNOLOGIES. He was the recipient of the 2002 Outstanding Graduate Research Advisor Award from the School of Electrical and Computer Engineering, Georgia Institute of Technology, and the 2003 Outstanding Faculty Leadership Award for the Mentoring of Graduate Research Assistants from the Georgia Institute of Technology. He is also the recipient of the 2003 Presidential Special Recognition Award from IEEE CPMT Society for his leadership of TC-12 and the IBM Faculty Award in 2004 and 2005. He has also served as a coauthor and Advisor for a number of Outstanding Student Paper Awards at EPEP '00, EPEP '02, EPEP '03, EPEP '04, ECTC '98, APMC '05, and the 1997 IMAPS Education Award. He is the recipient of the Shri. Mukhopadyay Best Paper Award at the International Conference on Electromagnetic Interference and Compatibility (INCEMIC), Chennai, India, 2003, the 2004 Best Paper Award in the IEEE TRANSACTIONS ON ADVANCED PACKAGING, the 2004 Commendable Paper Award in the IEEE TRANSACTIONS ON ADVANCED PACKAGING, and the Best Poster Paper Award at ECTC '04 and '06. In 2007, he and his students were recognized for their research by the Technical Excellence Award given by the Semiconductor Research Corporation (SRC) and Global Research Corporation (GRC).